Precise Fingerprint Determination of Vibrational Infrared Spectra in a Series of Co(II) Clathrochelates through Experimental and Theoretical Analyses

Angel Luis Corcho-Valdes, Josue Ponce de Leon-Cabrera, Ivan Padron-Ramirez, Frank Justo Chao-Mujica, Ekaterina Lebed, Alejandro Gutierrez-Quintanilla, Luis Felipe Desdin-Garcia, Yan Voloshin, Manuel Antuch

Precise fingerprint determination of vibrational infrared spectra in a series of Co(II) clathrochelates through experimental and theoretical analyses

Angel Luis Corcho-Valdes,[a] Josue Ponce de Leon-Cabrera,[a] Ivan Padron-Ramirez,[a] Frank Justo Chao-Mujica,[a] Ekaterina Lebed,[b,c] Alejandro Gutierrez-Quintanilla,[d] Luis Felipe Desdin-Garcia [a]*, Yan Voloshin,[b,c]* Manuel Antuch[a]*

[a] Centro de Aplicaciones Tecnologicas y Desarrollo Nuclear (CEADEN), No. 502, Calle 30 y 5ta Ave. Miramar, C.P. 11300 La Habana, Cuba.
[b] Nesmeyanov Institute of Organoelement Compounds of the Russian Academy of Sciences, 28-1 Vavilova st., 119334 Moscow, Russia.
[c] Kurnakov Institute of General and Inorganic Chemistry of the Russian Academy of Sciences, 31 Leninsky pr., 119991 Moscow, Russia.
[d] Université de Pau et des Pays de l'Adour, E2S UPPA, CNRS, IPREM, Pau, France

Manuel Antuch: 0000-0003-0007-7334; Luis Felipe Desdin-García: 0000-0003-4679-6019; Yan Voloshin: 0000-0003-2823-6560

Abstract

The energetic demands of modern society for clean energy vectors (such as H_2) have caused a surge in the research associated with homogeneous electrocatalysts that may replace Pt. In particular, clathrochelates have shown excellent electrocatalytic properties for the hydrogen evolution reaction (HER). However, the actual mechanism for the HER catalyzed by these important complexes remains an open debate, which may be addressed via Operando spectroelectrochemistry. The prediction of electrochemical properties via Density Functional Theory (DFT) needs access to thermodynamic functions, which are only available after Hessian calculations. Unfortunately, there is a notable lack in current literature regarding the precise evaluation of vibrational spectra of such complexes, given their structural complexity and the associated tangled IR spectra. In this work, we have performed a detailed theoretical and experimental analysis in a family of Co(II) clathrochelates, in order to establish univocally their IR pattern, and also the calculation methodology which is adequate for such predictions. In summary, we have observed the presence of multiple common bands shared by this organometallic family, using the B3LYP functional, the LANL2DZ basis and effective core potentials (ECP) for heavy atoms. The most important issue addressed in this article was therefore related to the detailed assignment of the fingerprint associated with Co(II) clathrochelates, which is a challenging endeavor due to the crowded nature of the spectra.

Keywords: macrocyclic compounds, clathrochelates, cobalt complexes, IR spectra, vibrational analysis, DFT.

1. Introduction

Energy is one of the main parts of human life and modern industry. Unfortunately, the energy crisis increases as a result of the decrease in the sources of fossil fuels.[1] Therefore, new and clean energy vectors are to be found nowadays. In this context H_2 is considered as a clean fuel that is potentially cost-effective because it comes from water or acidic aqueous solutions. The most promising cost-effective transitional metals used in hydrogen evolution reaction (HER) catalysts are Fe, Co, Ni, Cu, Mo and W. [2,3]

Cage complexes (for example, clathrochelates [4,5]) can be synthesized presenting Ni, Fe or Co as the transition metal ion of the molecule,[6–12] while the macrobicyclic cobalt(II) tris-α-dioximates (Scheme 1) allow the fabrication of a broad and interesting family of metal complexes. Such complexes have been highlighted[4,13] due to their efficiency as both homogeneous[14–19] and immobilized[20–23] electrocatalysts for hydrogen production. These are also reported to be good precatalysts for the deposition of highly catalytically-active metal[23–25]. Their three-dimensional macropolycyclic ligands with suitable electron-withdrawing substituents (especially halogen atoms) in their ribbed chelating ligand are able to stabilize the low (probably, catalytically active) oxidation states of their encapsulated transition metal ions (in particular, iron(I) and cobalt(I) oxidation states[20,26–28]), which makes them unique candidates to be applied as molecular electrocatalysts for the HER.[15,17]

Indeed, the plausible general catalytic cycle of the clathrochelate-electrocatalyzed HER[4,13] includes a formation of the cobalt (I, II, and III)-centered clathrochelate species. A detailed experimental study of their electronic structure has been performed,[29] along with their immobilization on top of Rh:$SrTiO_3$ photoelectrodes.[23] According to a previous report,[30] a cobalt clathrochelate with the most electron-withdrawing ribbed substituents has been found to have the lowest overpotential for the process of producing hydrogen via the $2H^+/H_2$ pathway. In this context, the use of combined theoretical Density Functional Theory (DFT) and spectral Electron paramagnetic resonance (EPR) and X-ray photoelectron spectroscopy (XPS) studies have proven useful[30–32] to assess the electronic structure of various cobalt clathrochelates.

Transition *d*-metal clathrochelates with encapsulated iron, ruthenium or cobalt(II) ion are especially promising electrocatalysts for the HER, when they are immobilized on the surface of the cathode of a given water electrolyser.[22] Surface functionalization *via* physisorption is reported[22] to be the easiest way to implement these macrobicyclic electrocatalysts and this process can be improved by increasing the number of polyaromatic groups per cage molecule of these complexes. Specifically, they can be adsorbed onto high-surface-area electrode materials and used as an alternative to metallic Pt-containing electrocatalysts. [13,22] However, the exact catalytic mechanism of the *d*-metal-electrocatalyzed HER in the case of the cobalt and iron complexes remains an open question.[24,25,33]

Theoretical studies of the resting cobalt(II) clathrochelates, are essential to shed light on the role of these complexes towards the HER.[31] Indeed, DFT has a strong predicting capability to provide clues for the improvement of various practical systems and industrial devices.[34–36] In particular, FTIR spectroscopy methods allow to study in detail the aforementioned clathrochelate monolayers, immobilized on a surface of various inorganic and organic supports (substrates), thus giving the innovative hybrid organo-inorganic materials.[12,17]

Although multiple DFT studies have been performed earlier to address the geometry and electronic structure of clathrochelates[25,30–32,37,38], a comprehensive and systematic theoretical description of their vibrational signature (characteristic normal modes and relative intensities of the bands), combined with a thorough comparison to their IR patterns has not been reported been to date. This work has therefore an importance that goes beyond the mere description of IR spectra, because the prediction of redox potentials needs the calculation of thermodynamic functions, which are available only after the calculation of the Hessian matrix. We aimed to apply high-level quantum-chemical methods to combine the experimental IR spectra of these cobalt(II) clathrochelates with known XRD structures (Scheme 1), thus providing a complete description of their normal modes of vibration. The analysis of *Operando* vibrational spectroscopy would require the precise knowledge of the normal modes of the selected complexes aiming at establishing the fingerprint of possible reactive intermediates.[39–42] The findings of this work would be useful for any future research regarding the vibrational spectroelectrochemistry of these compounds in *Operando* conditions, and also to establish a clear methodology to predict the geometry and the standard redox potentials of specific clathrochelate complexes. In summary, this work will set the experimental and theoretical bases for the future detailed description of *Operando* vibrational spectroscopy of Co clathrochelates under HER conditions.

2. Theoretical and experimental methods

2.1 Quantum-chemical calculations

The geometry of the cobalt(II)-centered clathrochelate molecules under study (Scheme 1) and their corresponding IR frequencies were theoretically calculated using the GAMESS program.[43,44] The B3LYP exchange correlation functional, and the LANL2DZ basis set of double-ξ quality with effective core potentials (ECP) for cobalt and chlorine atoms were employed.[45] The group $SCF was added to introduce Pulay's Direct inversion in the iterative subspace (DIIS) and Davidson's damping of the Fock matrix; moreover, DIIS was set from the beginning of the calculations using the ETHRSH keyword, and increasing the energy threshold for DIIS from 0.5 Hartree to 10 Hartree. Regarding the prediction of vibrational spectra, harmonic vibrational frequencies were computed for all these molecules via Hessian calculations. Hessian calculations are typically controlled via the

$FORCE group, and all their parameters were kept with their default values. All eigenvalues of the Hessian matrix were positive, indicating the structures were true minima. Anharmonic vibrational frequencies were computed for one of these molecules with the keyword RUNTYP=VSCF in the $CONTRL group. $HESS and $DIPDR groups were added to the input script from the previous harmonic calculations. In all our calculations of vibrational frequencies we have used a scaling factor of 1.00. All calculations reported herein were performed with a multiplicity of 2 for, which is the spin multiplicity observed experimentally at room temperature for Co clathrochelates[30] and therefore Restricted Open-Shell Kohn-Sham wavefunctions were employed. We have performed calculations in gas phase, in acetonitrile (AN) and in dimethylformamide (DMF), following the Polarizable Continuum Model - Solvation Model Density (PCM-SMD) formalism,[46] as implemented in GAMESS. PCM computes the interaction of electrostatic nature between the solvent treated as a continuum dielectric, and the wavefunction of the solute which is represented via its electron density. The classical PCM approach does not consider some contributions to the calculation of solvation energy, that comprise the energy associated to the creation of a hole in the solvent (known as cavitation energy) or the dispersion interactions between the solvent and the solute; these corrections are embodied in a parametric way in the SMD approach, as described in detail in the specialized literature.[46] A typical GAMESS input file is provided for Co(2+)@**L6** at the end of the supporting information.

Table 1. The types and the nature of the substituents at a diboron-capped cobalt(II)-centered tris-α-dioximate cage framework in the clathrochelate molecules under study

Complex	Apical (A)	Ribbed (R)
(Co^{2+})@L1	*meta*-C_6H_4COOH	$(CH_2)_4$
(Co^{2+})@L2	*n*-C_4H_9	$(CH_2)_4$
(Co^{2+})@L3	*n*-C_4H_9	H
(Co^{2+})@L4	*n*-C_4H_9	C_6H_5
(Co^{2+})@L5	*n*-C_4H_9	CH_3
(Co^{2+})@L6	F	CH_3
(Co^{2+})@L7	CH_3	Cl
(Co^{2+})@L8	C_6H_5	Cl
(Co^{2+})@L9	C_6F_5	Cl

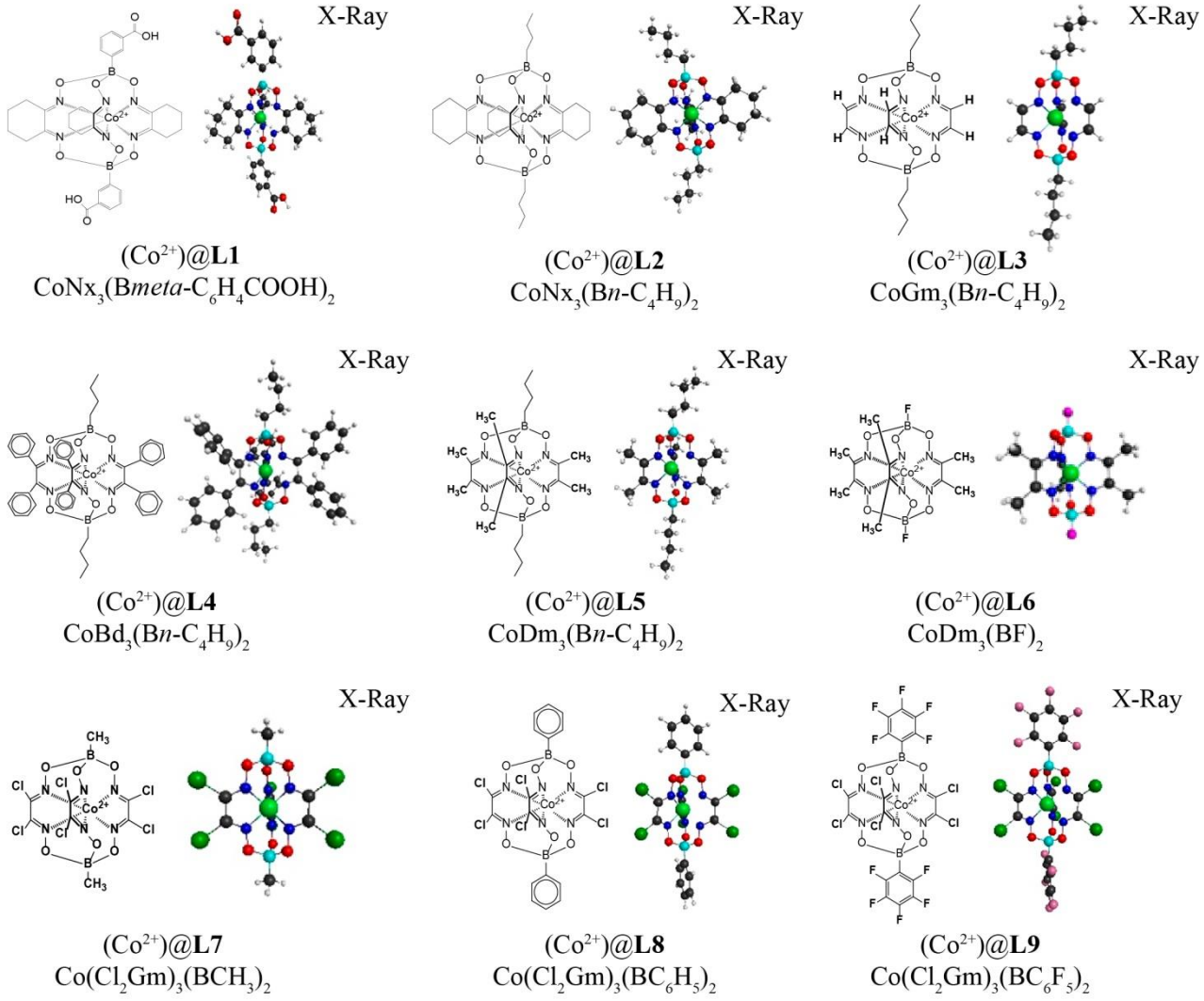

Scheme 1. Chemical drawings and the single crystal XRD structures obtained from the cobalt(II) complexes under study (For detailed XRD structures see Figure S1).

2.2 Materials and IR measurements

Cobalt(II) complexes under study with known XRD structures were prepared as described elsewhere.[47–50] IR spectra were recorded in the range 400 – 4000 cm^{-1} with a VERTEX 70v Fourier-transform IR spectrophotometer by the attenuated total reflection (ATR) method using a Pike Glady ATR adapter with a diamond crystal. The spectral resolution was equal to 4 cm^{-1} and each spectra was acquired after 64 scans. The spectra were directly obtained from the powder samples of the complexes under study without their pretreatment. Measured ATR spectra were corrected using the OPUS 7 software to treat the wavelength dependences of a radiation penetration depth into the sample.

3. Results and Discussion

Prediction of molecular geometries

Table 2 allows us to compare the DFT-calculated Co–N distances in the cobalt(II)-centered cage molecules under study with those experimentally XRD-obtained. Their low-spin Co^{2+} ion with electronic d^7 configuration is shifted from the centrum of its CoN_6-coordination polyhedron. Values of the intramolecular B···Co···B angle ψ, also compiled in this Table, were used to illustrate the Jan–Teller (*JT*) structural distortion. The obtained theoretical results were compared with the known XRD data, suggesting that the use of the B3LYP functional resulted in the slightly overestimated bond distances. Such as slight overestimation of Co-N bond distances was essentially the same after calculations in the gas phase, AN and DMF (Table S1), indicating that the simulation environment around the complex had negligible influence on the estimated structural parameters. The aforementioned structural effect, which can be also characterized by the value of ψ, caused a shift of the encapsulated Co^{2+} ion in a direction of one of the three chelate α-dioximate ligand fragments. As a result, the corresponding CoN4'N2''-coordination polyhedron is formed. This fact is adequately reproduced by calculations with the B3LYP functional. On the other hand, such *JT*-distorted geometry in the solid state is not necessary to be the same as that in solution. The X-ray structure of the (Co^{2+})@**L1** complex is not solved. However, Table 2 shows the excellent agreement between the experimental and the DFT-predicted Co-N bond distance; such an excellent agreement shows that our calculation methodology is adequate for the structural description of this family of complexes.

Table 2. Main calculated and experimental (in parentheses) geometrical parameters of a cage framework in the cobalt(II) clathrochelates under study.

	(Co^{2+})@L1	(Co^{2+})@L2	(Co^{2+})@L3	(Co^{2+})@L4	(Co^{2+})@L5	(Co^{2+})@L6	(Co^{2+})@L7	(Co^{2+})@L8	(Co^{2+})@L9
Co–N1 (Å)	2.16	2.16 (2.06)	2.15 (2.11)	2.17 (2.14)	2.15 (2.13)	2.15 (1.97)	2.15 (2.14)	2.16 (2.01)	2.16 (2.03)
Co–N2 (Å)	2.15	2.15 (2.02)	2.15 (2.10)	2.15 (2.10)	2.14 (2.12)	2.13 (1.97)	2.12 (2.14)	2.16 (2.01)	2.16 (2.03)
Co–N3 (Å)	1.97	1.97 (1.92)	1.97 (1.90)	2.00 (1.94)	1.98 (1.89)	2.00 (1.97)	1.96 (1.92)	1.99 (2.00)	1.99 (2.01)
Co–N4 (Å)	1.91	1.91 (1.88)	1.92 (1.90)	1.92 (1.89)	1.92 (1.89)	1.91 (1.97)	1.89 (1.90)	1.93 (1.99)	1.93 (1.96)
Co–N5 (Å)	1.91	1.91 (1.88)	1.92 (1.89)	1.93 (1.89)	1.92 (1.89)	1.93 (1.97)	1.93 (1.90)	1,93 (1.99)	1,93 (1.96)
Co–N6 (Å)	1.96	1.96 (1.89)	1.97 (1.90)	1.98 (1.93)	1.97 (1.89)	1.96 (1.97)	1.94 (1.92)	1.99 (2.00)	1.99 (2.01)
Ψ (B...Co...B) {deg}	172	172 (174)	173 (173)	174 (174)	173 (172)	174 (180)	174 (172)	173 (179)	173 (178)

Comparison of the experimental and theoretical (DFT) IR spectra

The experimental bands are summarized in Table 3 and in Table S2. The vibrational frequencies of clathrochelate molecules under study were calculated using the GAMESS program[48] and their IR spectra were subsequently processed with the Gabedit program (version 2.4.8).[51] The line spectra obtained from GAMESS were convolved in Gabedit using Lorenzian lineshapes using a full width at half maximum (FWHM) of 20 cm^{-1}.

Table 3. Compilation of selected normal modes for each clathrochelate studied in this work. Each normal mode may be classified as ring deformation (RD), wagging (W), scissors (S), rocking (R) and twisting (T).

Co@**L1**	Wavenumber (cm^{-1})	579	774	832	870	926	994	1061	1222	1263	1666
	Mode	γ_{N-O}	$\delta^{s}_{C=N}$ (S)	γ_{B-O} (W)	ν^{as}_{B-O}	δ^{s}_{N-O} (R)	δ_{B-O} (S)	ν_{N-O}	$\delta^{s}_{C=N}$ (R)	ν_{B-C}	$\nu_{C=O}$
Co@**L2**	Wave number (cm^{-1})	588	709	769	838	952	999	1061	1126	1407	1624
	Mode	γ_{N-O}	γ_{B-O} (T)	δ_{N-O} (T)	δ_{N-O} (R)	ν^{as}_{B-O}	δ_{N-O} (R)	ν_{N-O}	γB-O	νC=N	$\nu^{s}_{C=N}$
Co@**L3**	Wavenumber (cm^{-1})	698	830	942	1048	1115	1525	1639			
	Mode	γ^{s}_{B-O} (W)	γ_{B-O}	ν^{as}_{B-O}	νN-O	ν^{s}_{N-O}	νC=N	νC=N			
Co@**L4**	Wavenumber (cm^{-1})	511	713	810	859	926	953	1091	1340	1598	
	Mode	γ_{B-O} (W)	$\gamma_{C=N}$ (T)	γ_{B-O} (T)	δ_{B-O}	δ_{N-O} (S)	ν^{as}_{B-O}	νN-O	$\delta_{C=N}$ (S)	$\nu_{C=N}$	
Co@**L5**	Wavenumber (cm^{-1})	628	758	770	927	949	968	1093	1138	1633	
	Mode	γ_{B-O} (T)	δ^{as}_{B-O}	δ_{B-O}	δ^{s}_{N-O} (S)	ν^{as}_{B-O}	δ^{s}_{N-O}	ν_{B-O}	$\delta^{as}_{C=N}$ (S)	$\nu_{C=N}$	
Co@L6	Wavenumber (cm^{-1})	814	818	932	947	1095	1152	1646			
	Bond	δ_{B-O}	$\delta_{C=N}$	δ^{s}_{N-O} (S)	ν^{as}_{B-O}	ν_{N-O}	$\delta_{C=N}$	$\nu_{C=N}$			
Co@**L7**	Wavenumber (cm^{-1})	804	918	995	1132	1346	1600				
	Mode	δ_{B-O}	δ_{N-O} (S)	δ^{as}_{B-O}	ν_{N-O}	$\delta_{C=N}$	$\nu_{C=N}$				

Co@**L8**	Wavenumber (cm^{-1})	795	837	864	950	1018	1124	1264	1303	1599
	Mode	γ_{N-O} (T)	γ_{B-O}	γ_{B-O}	ν_{B-O}	δ^{s}_{N-O}	ν_{N-O}	ν_{B-C}	$\delta_{C=N}$ (S)	$\nu_{C=N}$
Co@**L9**	Wavenumber (cm^{-1})	730	855	881	908	1021	1119	1305	1602	
	Mode	γ_{B-O} (W)	γ_{B-O}	δ_{B-O}	δ_{N-O} (R)	ν_{N-O}	ν_{B-O}	$\delta_{C=N}$	$\nu_{C=N}$	

It is worth noting that their tangled structure suggests that anharmonic potentials might be necessary for their vibrational description. We proceeded then to calculate the IR spectra of a complex taking into account their anharmonicity. It is interesting the case of (Co^{2+})@**L3** where we observed an excellent agreement between the harmonic and anharmonic approximations, regarding the prediction of normal modes (see in Supplementary Information (SI) Figure S3). This shows that the harmonic approximation is enough for the vibrational description of clathrochelates; consequently, the rest of the analyses presented herein were performed under the harmonic approximation.

We further performed calculations in gas phase, AN and DMF with the selected complexes (Co^{2+})@**L8** and (Co^{2+})@**L9**. Figure S4 and S5 show the comparison of the predicted IR spectra in these three media, which were essentially the same and therefore we continued all our analyses using DMF as the surrounding medium for each complex. It is interesting to observe the excellent agreement between our theoretical approach and the experiment, considering that the experiment was performed in solid state and the theory was carried out with the discrete complex. It has been stated that the molecular environment in the solid state may be mimicked via the inclusion of continuum solvation, which proved to be successful in the framework of Mössbauer spectroscopy.[52] In our case, the agreement between experiment (in solid state) and theory (isolated molecule with and without continuum solvation) expresses that the normal modes are not affected by any supramolecular interaction between nearby complexes.

As an example, the normal modes of the cobalt(II)-centered cage framework (Co^{2+})@**L2** is depicted in Fig. 1. The comparison between the experimental spectrum and the calculated normal modes allowed us to assign the corresponding bands. The numbers from 1 to 10 represent the most intense normal modes corresponding to the observed experimental bands. The rest of the theoretical IR spectra of all cobalt(II) complexes under study are presented in SI section Figure S2. The corresponding wavenumber for each of the normal modes, and the mode assignment (main bonds involved and additional normal modes are compiled in Table S2). In the exampling clathrochelate molecule (Co^{2+})@**L2** shown Fig. 2 demonstrates a normal modes of the B–O bond in the tripodal cross-linking fragment of this macrobicyclic molecule that is coupled with the Csp^3–*H* bonds of its

cyclohexane ribbed moieties and of its *n*-butyl apical substituents at a cage framework as well. All the normal modes for each of the cobalt(II) clathrochelates under study are presented in SI section (Figure S6).

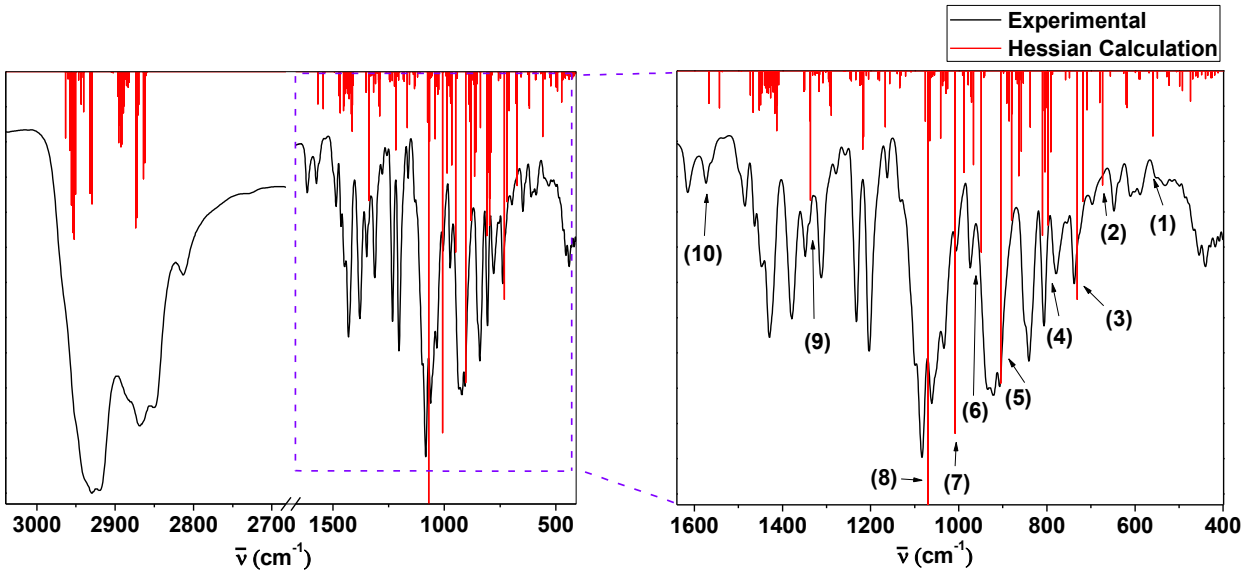

Figure 1. Comparison of the experimental and DFT-calculated IR spectra of the clathrochelate $CoNx_3(Bn\text{-}C_4H_9)_2$ {(Co^{2+})@L2}.

Analysis of IR spectra

The spectra contain the fingerprint bands characteristic of a given type of cage complexes, the similarities, and differences in the IR spectra of these macrobicyclic analogs can be analyzed. It is worth to express that the fingerprint region spans within the range 1500 and 500 cm^{-1}, but we will extend our analysis to the whole IR spectrum, bearing in mind that the less evident spectral assignments are involved with the fingerprint region. Based on the data compiled in Table 1, several comparisons for the clathrochelate molecules with the same apical or ribbed substituents (Figs. 3 – 6) can be made. All IR spectra can see in SI (Figure S2).

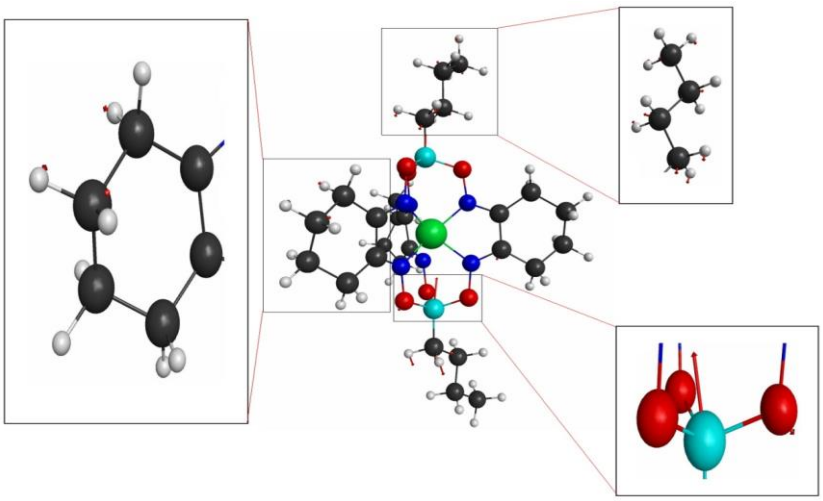

Figure 2. Example of a normal mode for the molecule $CoNx_3(Bn\text{-}C_4H_9)_2$ {(Co^{2+})@L2} at 1070 cm^{-1}. Its $\nu_{B–O}$ where the coupled $\delta_{Csp3–H}$ (A)+ $\delta_{Csp3–H}$ (R) normal modes may be observed.

In particular, the molecules (Co^{2+})@**L1** and (Co^{2+})@**L2** have the same ribbed substituents, but the different apical groups at their capping boron atoms. The values of main covalent bonds, as well as that of the angle ψ, are similar. Their common bands shown in Fig. 3 in the same macrobicyclic framework are $\gamma_{N–O}$ (579 – 588 cm^{-1}), $\gamma_{B–O}$ (709 – 832 cm^{-1}), $\nu_{B–O}$ (870 – 952 cm^{-1}), $\delta_{N–O}$ (926 – 999 cm^{-1}), $\nu_{N–O}$ (1061 cm^{-1}) and $\nu_{C=N}$ (1624 – 1666 cm^{-1}). Besides, these complexes belong to a broad family of the tris-α-dioximate clathrochelates sharing their IR spectra characteristic stretching and deformation vibrational bands related to their covalent N–O and C=N bonds, the spectrum of (Co^{2+})@**L1** also contains a unique signature, i.e. $\delta_{C=N}$ (774 and 1222 cm^{-1}), $\delta_{B–O}$ (994 cm^{-1}), $\nu_{B–C}$ (1263 cm^{-1}) and $\nu_{C=O}$ (1666 cm^{-1}) bands. IR spectrum of (Co^{2+})@**L2** contains the characteristic bands $\delta_{N–O}$ (769 and 838 cm^{-1}), $\gamma_{B–O}$ (1126 cm^{-1}) and $\nu_{C=N}$ (1407 and 1624 cm^{-1}).

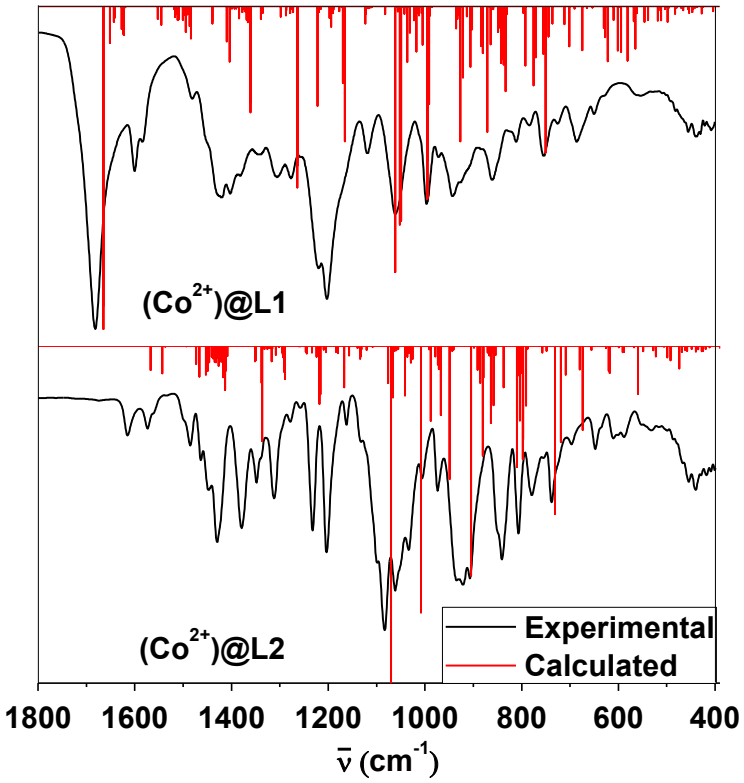

Figure 3. Comparison of the experimental and DFT-calculated IR spectra of the clathrochelates $CoNx_3(B\textit{mema}\text{-}C_6H_4COOH)_2$ {(Co^{2+})@L1} and $CoNx_3(B\textit{n}\text{-}C_4H_9)_2$ {(Co^{2+})@L2}.

Molecules (Co^{2+})@**L2**, (Co^{2+})@**L3**, (Co^{2+})@**L4** and (Co^{2+})@**L5** contain the same apical groups, but different ribbed substituents. As follows from the data compiled in Table 2 and Fig. 4. The IR spectrum of the complex (Co^{2+})@**L4** is blue-shifted, as compared with the spectra of other clathrochelates of this row (probably, because of the electromeric effect of its ribbed aromatic substituents). IR spectra of all of them contain three common stretching vibration bands $\boldsymbol{\nu_{B-O}}$ (942 – 953 cm^{-1}), $\boldsymbol{\nu_{N-O}}$ (1048 – 1091 cm^{-1}) and $\boldsymbol{\nu_{C=N}}$ (1598 – 1639 cm^{-1}). Those of the complexes (Co^{2+})@**L2**, (Co^{2+})@**L3** and (Co^{2+})@**L4** contain the common band of the same type, such as $\boldsymbol{\gamma_{B-O}}$ (698 – 810 cm^{-1}), while the spectra of (Co^{2+})@**L2**, (Co^{2+})@**L3** and (Co^{2+})@**L5** showed the common deformation band $\boldsymbol{\delta_{N-O}}$ in the range 926 – 999 cm^{-1}. Complexes (Co^{2+})@**L4** and (Co^{2+})@**L5** have the common stretching vibration band $\boldsymbol{\gamma_{B-O}}$ (511 – 628 cm^{-1}) and the deformation band $\boldsymbol{\delta_{C=N}}$ (1138 – 1340 cm^{-1}) as well. The spectrum of (Co^{2+})@**L3** contains the characteristic α-dioximate bands $\boldsymbol{\nu_{N-O}}$ (1115 cm^{-1}) and $\boldsymbol{\nu_{C=N}}$ (1525 cm^{-1}). In the case of (Co^{2+})@**L4**, its IR spectrum contains $\boldsymbol{\gamma_{C=N}}$ (713 cm^{-1}) and $\boldsymbol{\delta_{B-O}}$ (810 cm^{-1}), while that of (Co^{2+})@**L5** demonstrates a doubled deformation $\boldsymbol{\delta_{B-O}}$ (758 and 770 cm^{-1}) and stretching vibration $\boldsymbol{\nu_{B-O}}$ (1093 cm^{-1}) bands.

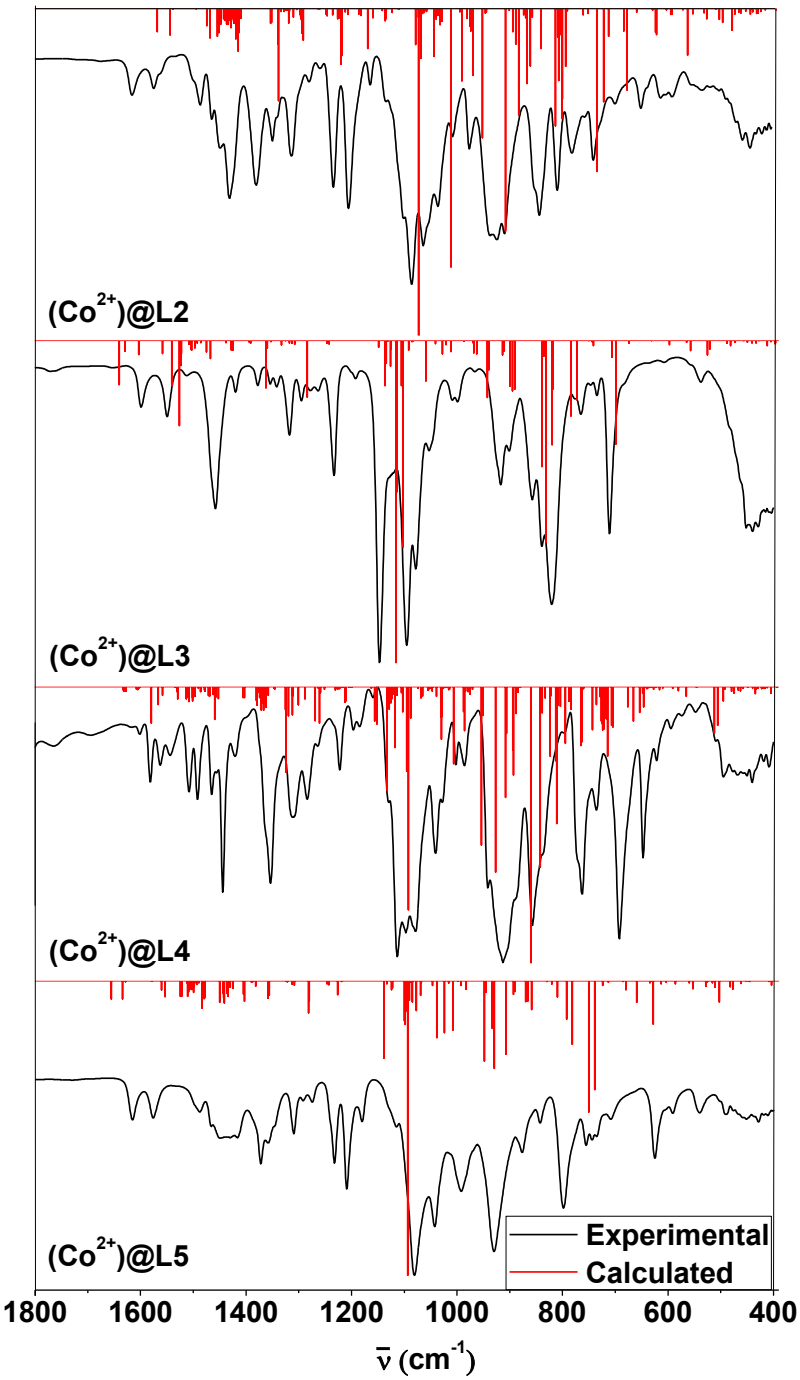

Figure 4. Comparison of the experimental and DFT-calculated IR spectra of the clathrochelates $CoNx_3(Bn\text{-}C_4H_9)_2$ {(Co^{2+})@L2}, $CoGm_3(Bn\text{-}C_4H_9)_2$ {(Co^{2+})@L3}, $CoBd_3(Bn\text{-}C_4H_9)_2$ {(Co^{2+})@L4} and $CoDm_3(Bn\text{-}C_4H_9)_2$ {(Co^{2+})@L5}.

The molecules (Co^{2+})@**L5** and (Co^{2+})@**L6** have the same ribbed substituents, but different apical groups. The position of the stretching vibration and deformation bonds, characteristic of their cage framework, are similar; the values of their angle ψ are also similar. The corresponding IR spectra shown in Fig.5 contain the common bands $\boldsymbol{\delta_{B-O}}$ (758 – 814 cm^{-1}), $\boldsymbol{\delta_{N-O}}$ (927 – 968 cm^{-1}), $\boldsymbol{\nu_{B-O}}$ (947 – 949 cm^{-1}), $\boldsymbol{\delta_{C=N}}$ (1138– 1152 cm^{-1}) and $\boldsymbol{\nu_{C=N}}$ (1633– 1646 cm^{-1}). The spectrum of (Co^{2+})@**L5** also

contains one more deformation band γ_{B-O} at 628 cm^{-1}. The spectrum of (Co^{2+})@**L6** also contains one more deformation band $\delta_{C=N}$ at 818 cm^{-1}.

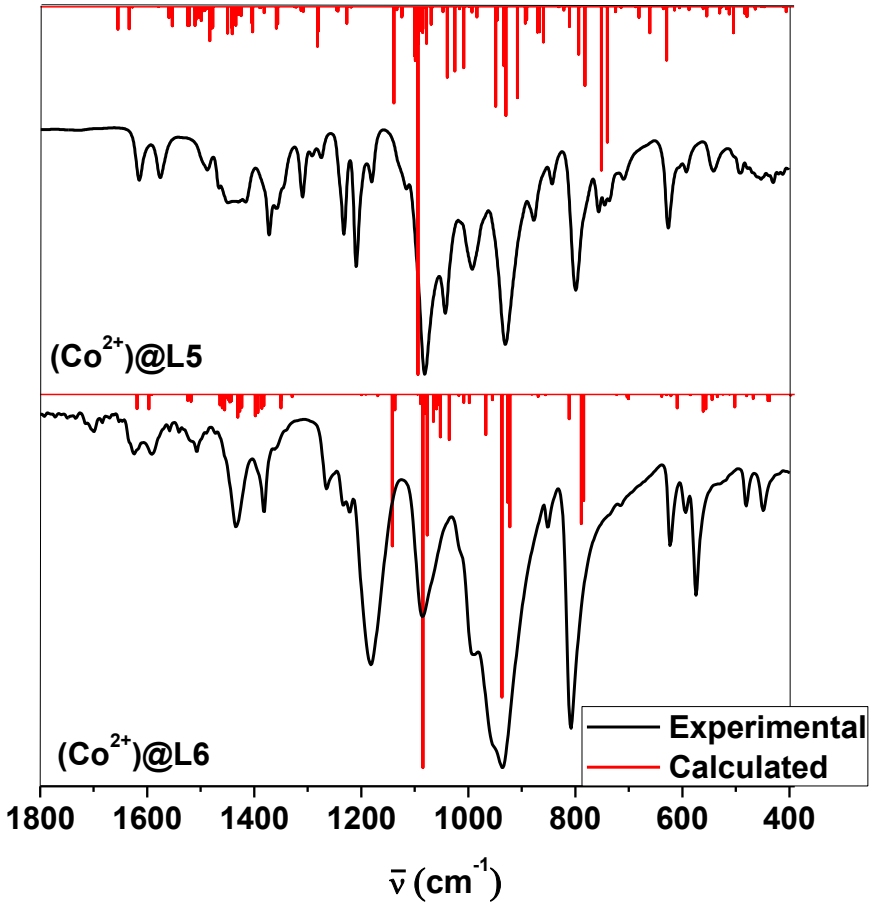

Figure 5. Comparison of the experimental and DFT-calculated IR spectra of the clathrochelates $CoDm_3(Bn\text{-}C_4H_9)_2$ {(Co^{2+})@L5} and $CoDm_3(BF)_2$ {(Co^{2+})@L6}.

Clathrochelates (Co^{2+})@**L7**, (Co^{2+})@**L8** and (Co^{2+})@**L9** have the same ribbed groups, but the different substituents in their chelating α-dioximate fragments. The main bands in the IR spectrum of the complex (Co^{2+})@**L7** are slightly shifted to the high frequency region, as compared with those of other aforementioned clathrochelates (Table 2 and Fig. 6). This fact can be caused, probably, by the inductive effect of its apical methyl groups (the Tuft's σ_I constant for this group is equal to –0.05), whereas those for the aromatic C_6H_5- and C_6F_5- groups are positive (+0.10 and +1.50, respectively). Their IR spectra contain the common bands δ_{N-O} (908 – 1018 cm^{-1}), ν_{N-O} (1021 – 1132 cm^{-1}), $\delta_{C=N}$ (1303 – 1346 cm^{-1}) and $\nu_{C=N}$ (1599 – 1602 cm^{-1}). Those of (Co^{2+})@**L7** and (Co^{2+})@**L9** showed the common deformation band δ_{B-O} in the range 881 – 995 cm^{-1}. The spectra of (Co^{2+})@**L8** and (Co^{2+})@**L9** have the common characteristic stretching vibration bands γ_{B-O} (730 – 837 cm^{-1} and 855 – 864 cm^{-1}), while that of (Co^{2+})@**L7** contains its own deformation band δ_{B-O} at 804 cm^{-1}. IR spectrum of (Co^{2+})@**L8** also contains the characteristic stretching vibration bands γ_{N-O} (795 cm^{-1}), γ_{B-O} (864 cm^{-1}), ν_{B-O} (950 cm^{-1}) and ν_{B-C} (1264 cm^{-1}). Those for the complex

(Co^{2+})@**L9** are γ_{B-O} (855 cm^{-1}) and ν_{B-O} (1119 cm^{-1}). A doubling of each of the stretching vibration or deformation IR band, assigned to the boron-containing bond, should be noted. This effect is probably caused by the presence of amounts of 20/80 of its two natural isotopes.

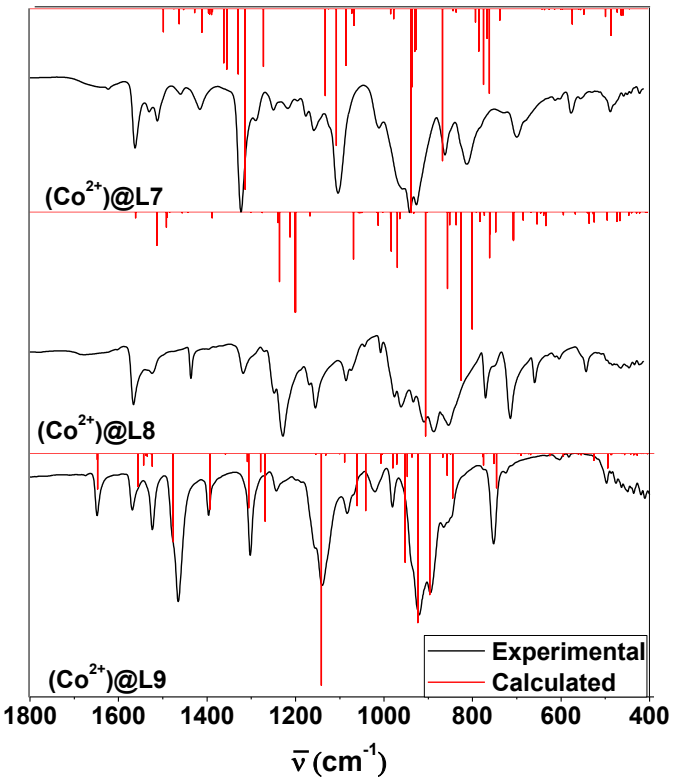

Figure 6. Comparison of the experimental and DFT-calculated IR spectra of the clathrochelates $Co(Cl_2Gm)_3(BCH_3)_2$ {(Co^{2+})@L7}, $Co(Cl_2Gm)_3(BC_6H_5)_2$ {(Co^{2+})@L8} and $Co(Cl_2Gm)_3(BC_6F_5)_2$ {(Co^{2+})@L9}.

In the case of IR spectra of the macrobicyclic cobalt(II) tris-nioximates (Co^{2+})@**L1** and (Co^{2+})@**L2**, the position of γ_{N-O} for the latter *n*-butylboron-capped complex is slightly higher than that in the spectrum of its analog with apical aromatic groups because the molecule (Co^{2+})@**L2** has a higher number of the coupled vibrations. Comparing the IR spectra of the complexes (Co^{2+})@**L2** and (Co^{2+})@**L3**, the stretching vibration $\nu_{C=N}$ for the former clathrochelate has a slightly higher value because the coupled vibrations are absent in the molecule (Co^{2+})@**L3**, whereas those with $\delta_{H-C=N}$ are present. In the case of the complexes (Co^{2+})@**L4** and (Co^{2+})@**L5**, the wavenumber of γ_{B-O} in the spectrum of the cobalt(II) tris-dimetylglyoximate (Co^{2+})@**L5** is higher because of a higher number of the coupled vibrations.

In the case of (Co^{2+})@**L5** and (Co^{2+})@**L6**, δ_{B-O} both present the common CH_3 group as ribbed substituent. However, in the case of (Co^{2+})@**L5** the mode with the lowest value because the n-butyl group presents a higher reduced mass of the mode. Regarding (Co^{2+})@**L6**, it could be due to an inductive electronic effect by the halogen (F), increasing the strength of the bond constant and the

wavenumber respectively.

Comparing the spectra of (Co^{2+})@**L8** and (Co^{2+})@**L9**, a slightly higher value of γ_{B-O} in the spectrum of the latter complex, as compared with that of the former clathrochelate**,** can be explained by the strong electron-withdrawing effect of the apical perfluoroaryl substituents in the molecule (Co^{2+})@**L9.** This caused an increase in the corresponding bond strength constant.

The calculation of IR spectra has been undertaken before in the literature with other basis sets and functionals. See Table S3 for a compilation of previous work regarding this endeavor. A comparison of our results to those presented in Table S3 shows that the use of scaling factors different than 1.00 remains a necessity in multiple cases, and that the harmonic approximation remains the dominant approach to predict vibrational normal modes. Moreover, basis sets of double-ξ quality are adequate in many systems for Hessian calculations.

As expressed in the introduction, the calculation of IR spectra permits to estimate the absolute thermodynamic functions for a precise oxidation state. In order to predict the redox potential of a species between two oxidation states the following expression applies

$$E^0_{abs}(O|R) = \frac{-\Delta G^0_{abs}(O|R)}{nF} \qquad (1)$$

Where $E^0_{abs}(O|R)$ is the absolute redox potential for the transformation $O + ne^- = R$; $\Delta G^0_{abs}(O|R)$ represents the absolute Gibbs free energy change for such redox reaction; F is the constant of Faraday and n represents the number of exchanged electrons.

Such $E^0_{abs}(O|R)$ must be referred to a reference reaction, which may be performed in different ways: some researchers refer to theoretical value of $E^0_{abs}(O|R)$ to the absolute potential of the Standard Hydrogen Electrode (SHE), but this approach has the disadvantage of the different values that such value presents in the literature, within the range of 4.281[53] to 4.44[54] V. This shows that the mere selection of the reference may introduce an error of 200 mV in the estimation. Other authors choose to calibrate their computational approach by optimizing a molecule (typically ferrocene, i.e., the $Fc|Fc^+$ couple) at the same level of theory than the $O|R$ couple and use equation 1 to predict a theoretical $E^0_{abs}(Fc|Fc^+)$; then the predicted redox potential $E^0_{abs}(O|R)$ is referred to the $E^0_{abs}(Fc|Fc^+)$ which permits to know if $E^0_{abs}(O|R)$ is positive or negative with regard to $E^0_{abs}(Fc|Fc^+)$ and how much.[31] In the case of non-aqueous electrochemistry and the use of aqueous references, appropriate account of the liquid junction potential is essential as well. A third approach is to compute Born-Haber cycles of gaseous and solvent-optimized structures in different redox states,[55,56] thereby giving access to $-\Delta G^0_{abs}(O|R)$. Providing further details falls outside the scope of the present work, but excellent and comprehensive reviews exist[57] and the interested reader is invited to delve into specific literature.[58,59]

In summary, the pattern shown in Fig. 7 was obtained by analyzing of IR spectra of all the cobalt(II)

clathrochelates under study (Table 1), of their calculated normal modes ~~(Table S2)~~, and of all the aforementioned information and its explanations. It is worth to highlight the agreement between experiment, performed in solid state, and theory, calculated in a DMF environment. This might suggest that the clathrochelates do not suffer important structural distortions upon their dissolution in DMF, but such assertion needs to be supported by experimental IR determinations in DMF.

The γ_{B-O} modes (shown in magenta) fall in the range 698 – 837 cm^{-1}, maxima of δ_{B-O} (shown in orange) are in the ranges 758 – 814 cm^{-1} and 859 – 995 cm^{-1}, while those of ν_{B-O} (shown in active blue) are between 870 and 953 cm^{-1}. Maxima of δ_{N-O} (shown in wine) are between 908 and 1018 cm^{-1} and those of ν_{N-O} (shown in dark yellow) fall in the range 1048 – 1132 cm^{-1}. The deformation vibration band $\delta_{C=N}$ (shown in blue) is found between 1138 and 1346 cm^{-1}, while maxima of $\nu_{C=N}$ (shown in olive) fall in the range 1598 – 1666 cm^{-1}. The most important finding of this work is therefore the precise determination of the fingerprint of Co(II) clathrochelates, as depicted in Figure 7.

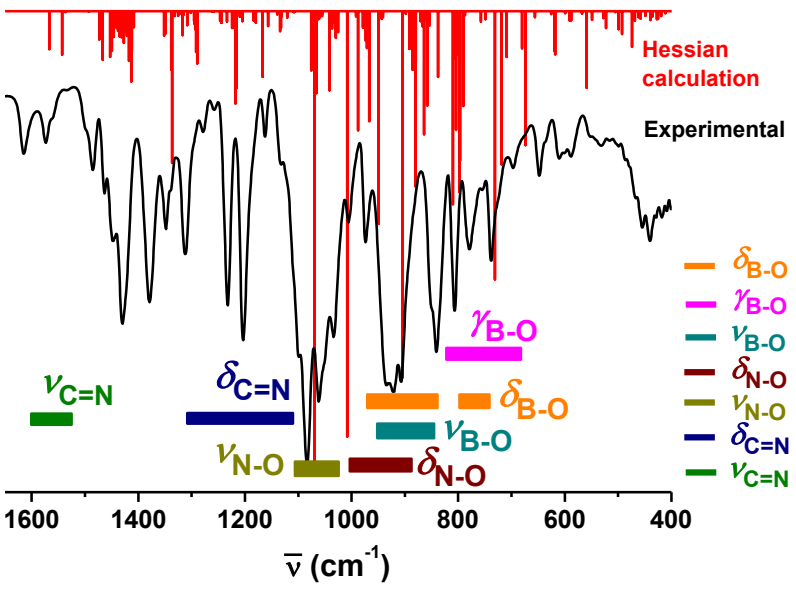

Figure 7. Fingerprint zone magnification (1500 and 500 cm^{-1}) with amide I and amide II regions of the IR spectrum of the clathrochelate $CoNx_3(Bn\text{-}C_4H_9)_2$ {(Co^{2+})@L2} where the ranges of typical normal modes are highlighted.

Certainly, future work with the purpose to strengthen our computational methodology will be directed to the theoretical prediction of clathrochelates and pseudoclathrochelates[60] having not only Co as the metal, but also Fe and Ru. Other ligands would be interesting to test, such as derivatives of the pseudomacrobicyclic tris-pyrazoloximate, tris-pyridylate analogs, boron-monocapped tris-a-dioximate analogs or encapsulating tris-diiminate ligands. Likewise, different redox states, namely I, II and III will be studied, thereby allowing to computation the redox potentials of these complexes

and also reorganization energies.[61–63] We will pay particular attention to the possibility of the participation of ligands in electron transfer processes and electrocatalysis, which is known as *ligand non-innocence*.[64–66] Future work may well be directed to the fingerprint assessment of redox states in non-resting conditions, and the comparison between different multiplicities since, for example, Co(I) may be a singlet or a triplet, Co(II) may be a doublet or a quartet and Co(III) a singlet or a quintet. Finally, it would be of interest to establish how the vibrational modes of clathrochelates would be modified under HER *Operando* conditions, and the coupling of such theoretical predictions to experimental measurements is of utmost importance.

It is worth to further highlight that this work demonstrates that the B3LYP/LANL2DZ combination provides accurate geometrical and vibrational predictions; but this does not implies that such methodology is general for any other applications. For example, beyond the HER, the use of clathrochelates as dyes for photovoltaic devices has not been performed yet, and in such context the prediction of UV Vis spectra is essential. We have shown, for example, that for TDDFT, the use of the B3LYP/LANL2DZ geometries but a combination of aug-cc-pVTZ for Co and cc-pVDZ for the rest of the molecule, thus permitting an adequate prediction of electronic spectroscopies.[67] On the other hand, the use of XRD data (whose geometry has been shown here and previously to be accurately predicted via the B3LYP/LANL2DZ combination[31]) with a large set of functionals (OLYP, RPBE, B3LYP, TPSS, BP86) and the Ahlrich's TZV basis was excellent in predicting electron densities at Fe nuclei and therefore trends in Mossbauer spectra.[60]

4. Conclusions

The FTIR spectra of a series of the cobalt(II) clathrochelates with known XRD structures have been recorded. Their molecular geometries were quantum-chemically optimized using the B3LYP functional and the LANL2DZ basis set, while the corresponding vibrational normal modes were theoretically calculated using Hessian calculations. Quantum-chemically calculated Co–N distances in their quasi-aromatic cage frameworks were compared to experimental XRD, where an excellent agreement was observed. IR spectra of the clathrochelate analogs and homologs with same apical or ribbed substituents at a cage framework were compared to observe the presence of common bands and the corresponding normal modes. We have studied a set of 9 clathrochelates presenting a variety of substituents; namely –*meta*–C_6H_4COOH, –*n*-C_4H_9, –F, $–CH_3$, $–C_6H_5$ and $–C_6F_5$ in the apical position while the ribbed positions spanned as substituents $–(CH_2)_4–$, –H, $–C_6H_5$, $–CH_3$ and –Cl. Our attention to the fingerprint region of such family of molecules allowed to conclude that (i) the region between 600 and 800 cm^{-1} was dominated by several normal modes associated to the B-O bonds; (ii) between 800 cm^{-1} and 1100 cm^{-1} there is a predominance of N-O bonds but δ_{B-O} appeared in the range between 800 and 1000 cm^{-1}; (iii) between 1100 and 1300 cm^{-1} the predominance was associated to $\delta_{C=N}$ and

(iv) right in the border with amide regions the $\nu_{C=N}$ was noticeable between 1500 and 1600 cm^{-1}. We have found that the harmonic approximation is enough to account for the theoretical prediction of IR spectra in a broad family of clathrochelates, which is remarkable given the inherent structural complexity of these molecules. This detailed knowledge sets an important precedent regarding the position of precise bands within the crowded IR spectra of Co(II) clathrochelates. Indeed, the calculation of normal modes plays a key role in the theoretical calculation of thermodynamic functions (Gibbs free energies and so on) via the sum of the energies associated to each normal mode. Therefore, the accurate prediction of IR spectra finds applications in electrochemistry since the DFT prediction of redox potentials include not only the consideration of electronic energy (nuclei-electron attraction and electron-electrons and nucleus-nuclei repulsion), but also zero-point energy correction and the thermodynamic functions, available only after Hessian calculations. In summary, this contribution sets a clear theoretical methodology (B3LYP functional, LANL2DZ basis set and ECP for heavy atoms; Co and Cl) not only for the structural description of this family of cage complexes, but also for the precise calculation of redox potentials of electrocatalytically-active species, in addition to the assessment of specific fingerprints of vibrational spectra.

Supporting information

Structure of the nine clathrochelates studied in this work. Comparison among experimental Co-N bond distances for selected complexes in different media. Exhaustive compilation of normal modes. Other methodologies available in the literature used to predict normal modes. Plots of Theoretical vs. calculated vibrational spectra of Co@L1 to Co@L9. Armonic vs. anharmonic approximation for Co@L3. Hessian calculation of Co(2+)@L8 and Co(2+)@L9 in acetonitrile (AN), dimethylformamide (DMF) and in gas phase. Depiction of selected normal modes for each molecule.

Acknowledgements

The synthesis of clathrochelate complexes and IR measurements were supported by the Ministry of Science and Higher Education of the Russian Federation (Contract No. 075-03-2023-642). The authors wish to gratefully thank the “Empresa Cubana de Navegación Aérea (ECNA)” and its “Laboratorio de Investigaciones de Tecnologías Aeronáuticas (LITA)” for providing critical computational infrastructure to perform the DFT calculations. In particular, the authors are warmly thankful to Fernando Iglesias, Osvaldo Pagés Brillante, Ronald Aneiro Mir, Julio César Desten Anaya, Jenny Martínez Delgado, Arlet Torres Carballosa and Irán Hormigó Puertas for their kind availability to create excellent computational conditions. Manuel Antuch is thankful to Pierre Millet, who provided also computational infrastructure for some of the calculations presented in this work.

Conflicts of interest

The authors declare no conflict of interest.

References

(1) Gates, B. *How to Avoid a Climate Disaster : Solutions We Have and the Breakthroughs We Need*, 1st ed.; Knopf, 2021.

(2) Abe, J. O.; Popoola, A. P. I.; Ajenifuja, E.; Popoola, O. M. Hydrogen Energy, Economy and Storage: Review and Recommendation. *Int. J. Hydrogen Energy* **2019**, *44*, 15072–15086. https://doi.org/10.1016/j.ijhydene.2019.04.068.

(3) Vos, S. D. De; Otten, M.; Wissink, T.; Broere, D. L. J.; Hensen, E. J. M.; Klein, R. J. M. Hydrogen Evolution Electrocatalysis with a Molecular Cobalt Bis (Alkylimidazole) Methane Complex in DMF : A Critical Activity Analysis. **2022**, *202201308*, 1–8. https://doi.org/10.1002/cssc.202201308.

(4) Voloshin, Y. Z.; Kostromina, N. A.; Krämer, R. *Clathrochelates: Synthesis, Structure and Properties*; Elsevier Science, 2011.

(5) Voloshin, Y.; Belaya, I.; Krämer, R. *Cage Metal Complexes Clathrochelates Revisited*, 1st ed.; Springer Cham, 2017. https://doi.org/10.1007/978-3-319-56420-3.

(6) Belov, A. S.; Novikov, V. V; Vologzhanina, A. V. Synthesis, Crystal Polymorphism and Spin Crossover Behavior of the Adamantylboron-Capped Cobalt (II) Hexachloroclathrochelate and Its Transformation into the CoIII CoII CoIII -Bis-Macrobicyclic Derivative. *Dalt. Trans.* **2023**, *52*, 347–359.

(7) Belov, A. S.; Belova, S. A.; Efimov, N. N.; Zlobina, V. V; Novikov, V. V; Nelyubina, Y. V; Zubavichus, Y. V; Voloshin, Y. Z.; Pavlov, A. A. Synthesis, X-Ray Structure and Magnetic Properties of the Apically Functionalized Monocapped Cobalt(Ii) Tris-Pyridineoximates Possessing SMM Behaviour. *Dalt. Trans.* **2023**, *52* (10), 2928–2932. https://doi.org/10.1039/D2DT04073E.

(8) Belova, S. A.; Belov, A. S.; Efimov, N. N.; Pavlov, A. A. Synthesis , Structure , and Magnetic Properties of Ditopic Ferrocenylboron-Capped Tris-Pyridineoximate Iron , Cobalt , and Nickel (II) Pseudoclathrochelates. **2022**, *67* (8), 1151–1157. https://doi.org/10.1134/S0036023622080034.

(9) Wei, Y.; Dong, Y.; Sun, W.; Hou, Q.; Shi, Q.; Lan, X. Phase Behavior and Heat Capacity of Alkylboron-Capped Cobalt (II) and Nickel (II) Clathrochelates. *Thermochim. Acta* **2022**, *716*, 179304. https://doi.org/https://doi.org/10.1016/j.tca.2022.179304.

(10) Chuprin, A. S.; Pavlov, A. A.; Vologzhanina, A. V; Dorovatovskii, P. V; Makarenkov, A. V; Ol'shevskaya, V. A.; Dudkin, S. V; Voloshin, Y. Z. Multistep Synthesis and X-Ray Structures of Carboxyl-Terminated Hybrid Iron(Ii) Phthalocyaninatoclathrochelates and Their Postsynthetic Transformation into Polytopic Carboranyl-Containing Derivatives. *Dalt. Trans.* **2023**, *52* (12), 3884–3895. https://doi.org/10.1039/D3DT00076A.

(11) Chuprin, A. S.; Dudkin, S. V; Belova, S. A.; Lebed, E. G.; Dorovatovskii, P. V; Vologzhanina, A. V; Voloshin, Y. Z. Synthesis and Reactivity of the Apically Functionalized (Pseudo)Macrobicyclic Iron(Ii) Tris-Dioximates and Their Hybrid Phthalocyaninatoclathrochelate Derivatives Comprising Reactive and Vector Terminal Groups. *New J. Chem.* **2022**, *46* (22), 10863–10877. https://doi.org/10.1039/D2NJ01560A.

(12) Shetty, S.; Idrees, K. B.; Xie, H.; Alameddine, B.; Farha, O. K. Synthesis of Zirconium-Based Metal–Organic Frameworks with Iron(II) Clathrochelate Ligands. *CrystEngComm* **2023**, *25* (10), 1550–1555. https://doi.org/10.1039/D2CE01686A.

(13) Voloshin, Y. Z.; Buznik, V. M.; Dedov, A. G. New Types of the Hybrid Functional Materials Based on Cage Metal Complexes for (Electro) Catalytic Hydrogen Production. *Pure Appl. Chem.* **2020**, *92*, 1159–1174.

(14) Pantani, O.; Naskar, S.; Guillot, R.; Millet, P.; Anxolabéhère-Mallart, E.; Aukauloo, A. Cobalt Clathrochelate Complexes as Hydrogen-Producing Catalysts. *Angew. Chem. Int. Ed. Engl.* **2008**, *47* (51), 9948–9950. https://doi.org/10.1002/anie.200803643.
(15) Voloshin, Y. Z.; Dolganov, A. V; Varzatskii, A.; Bubnov, Y. N. Efficient Electrocatalytic Hydrogen Production from H+ Ions Using Specially Designed Boron-Capped Cobalt Clathrochelates. *Chem. Comm.* **2011**, *47*, 7737–7739. https://doi.org/10.1039/c1cc12239h.
(16) Vologzhanina, A. V; Mokhir, A.; Bubnov, N.; Voloshin, Y. Z. Iron vs. Cobalt Clathrochelate Electrocatalysts of HER: The First Example on a Cage Iron Complex. *Dalt. Trans.* **2013**, *42*, 4373–4376. https://doi.org/10.1039/c3dt33073g.
(17) Vologzhanina, A. V; Romanenko, G. V; Budnikova, Y. G.; Zelinskii, G. E.; Buzin, I.; Voloshin, Y. Z. First Iron and Cobalt (II) Hexabromoclathrochelates: *Dalt. Trans.* **2015**, *44*, 2476–2487. https://doi.org/10.1039/c4dt03082f.
(18) Potapova, T. V; Vologzhanina, A. V; Varzatskii, O. A.; Bubnov, N. Apically Linked Iron(II) α-Dioximate and α-Oximehydrazonate Bis-Clathrochelates: Synthesis, Structure and Electrocatalytic Properties. *Dalt. Trans.* **2013**, *42*, 13667–13678. https://doi.org/10.1039/c3dt50881a.
(19) Dolganov, A. V; Belaya, I. G.; Voloshin, Y. Z. Electrochimica Acta Binuclear Iron (II) Cage Complexes as Electrocatalysts of Hydrogen Evolution Reaction in Different Hydrogen-Producing Systems. *Electrochim. Acta* **2014**, *125*, 302–306. https://doi.org/10.1016/j.electacta.2014.01.060.
(20) Voloshin, Y. Z.; Novikov, V. V; Nelyubina, Y. V; Belov, A. S.; Roitershtein, D. M.; Savitsky, A.; Mokhir, A.; Miehlich, M. E.; Meyer, K. Synthesis and Characterization of an Fe (I) Cage Complex with High Stability towards Strong H-Acids. *Chem. Commun.* **2018**. https://doi.org/10.1039/c7cc09611a.
(21) Voloshin, Y. Z.; Chornenka, N. V; Belov, A. S.; Grigoriev, S. A.; Pushkarev, A. S.; Millet, P.; Kalinichenko, V. N.; Belaya, I. G.; Bugaenko, M. G.; Dedov, A. G. Spectrophotometrical Study of the Physisorption of Iron (II) Clathrochelates Containing Terminal Phenanthrenyl Group (s) on Carbon Paper. *Macroheterocycles* **2018**, *11*, 449–453. https://doi.org/10.6060/mhc181008v.
(22) Voloshin, Y. Z.; Chornenka, N. V; Belov, A. S.; Grigoriev, S. A.; Pushkarev, A. S.; Millet, P.; Kalinichenko, V. N.; Oranskiy, D. A.; Dedov, A. G. Preparation and Electrochemistry of Iron , Ruthenium , and Cobalt (II) Hexaphenanthrene Clathrochelates Designed for Efficient Electrocatalytic Hydrogen Production and Their Physisorption on Carbon Materials. **2019**, *166* (13), 598–607. https://doi.org/10.1149/2.0391913jes.
(23) Cheikh, J. Al; Villagra, A.; Ranjbari, A.; Pradon, A.; Antuch, M.; Dragoe, D.; Millet, P.; Assaud, L. Engineering a Cobalt Clathrochelate/Glassy Carbon Interface for the Hydrogen Evolution Reaction. *Appl. Catal. B Environ.* **2019**, *250*, 292–300. https://doi.org/10.1016/j.apcatb.2019.03.036.
(24) Anxolabéhère-Mallart, E.; Costentin, C.; Fournier, M.; Nowak, S.; Robert, M.; Savéant, J. M. Boron-Capped Tris(Glyoximato) Cobalt Clathrochelate as a Precursor for the Electrodeposition of Nanoparticles Catalyzing H2 Evolution in Water. *J. Am. Chem. Soc.* **2012**, *134* (14), 6104–6107. https://doi.org/10.1021/ja301134e.
(25) Ghachtouli, S. El; Fournier, M.; Cherdo, S.; Guillot, R.; Charlot, M.-F.; Anxolabéhère-Mallart, E.; Robert, M.; Aukauloo, A. Monometallic Cobalt − Trisglyoximato Complexes as Precatalysts for Catalytic H2 Evolution in Water. *J. Phys. Chem. C* **2013**, *117*, 17073–17077.
(26) Voloshin, Y. Z.; Varzatskii, O. A.; Vorontsov, I. I.; Antipin, M. Y. Tuning a Metal s Oxidation State: The Potential of Clathrochelate Systems. *Angew. Chem. Int. Ed.* **2005**, *44*, 3400–3402. https://doi.org/10.1002/anie.200463070.
(27) Voloshin, Y. Z.; Varzatskii, O. A.; Novikov, V. V; Strizhakova, N. G.; Vorontsov, I. I.; Vologzhanina, A. V; Lyssenko, K. A.; Romanenko, G. V; Fedin, M. V; Ovcharenko, V. I.; Bubnov, Y. N. Tris-Dioximate Cobalt (I , II , III) Clathrochelates : Stabilization of Different Oxidation and Spin States of an Encapsulated Metal Ion by Ribbed Functionalization. **2010**,

5401–5415. https://doi.org/10.1002/ejic.201000444.
(28) Zelinskii, G. E.; Pavlov, A. A.; Belov, A. S.; Belaya, I. G.; Vologzhanina, A. V; Nelyubina, Y. V; Nikolay, N. E.; Zubavichus, Y. V; Bubnov, Y. N.; Novikov, V. V; Voloshin, Y. Z. A New Series of Cobalt and Iron Clathrochelates with Per Fl Uorinated Ribbed Substituents. **2017**, 6852–6862. https://doi.org/10.1021/acsomega.7b01088.
(29) Kochubey, D. I.; Kaichev, V. V; Saraev, A. A.; Tomyn, S. V; Belov, A. S.; Voloshin, Y. Z. Combined X-Ray Absorption Near Edge Structure and X-Ray Photoelectron Study of the Electrocatalytically Active Cobalt (I) Cage Complexes and the Clathrochelate Cobalt (II) - and Cobalt (III) -Containing Precursors and Analogs. **2013**, No. I. https://doi.org/10.1021/jp3085606.
(30) Antuch, M.; Ranjbari, A.; Grigoriev, S. A.; Al-Cheikh, J.; Villagrá, A.; Assaud, L.; Voloshin, Y. Z.; Millet, P. Effect of the Ligand Framework of Cobalt Clathrochelates on Hydrogen Evolution Electrocatalysis: Electrochemical, Spectroscopic and Density Functional Theory Analyses. *Electrochim. Acta* **2017**, *245*, 1065–1074. https://doi.org/10.1016/j.electacta.2017.03.005.
(31) Antuch, M.; Millet, P. Approach to the Mechanism of Hydrogen Evolution Electrocatalyzed by a Model Co Clathrochelate: A Theoretical Study by Density Functional Theory. *ChemPhysChem* **2018**, *19*, 2549–2558. https://doi.org/https://doi.org/10.1002/cphc.201800383.
(32) Antuch, M.; Millet, P. The Use of Density Functional Theory to Decipher the Electrochemical Electrochemical Activity Activity of of Metal Metal Clathrochelates Clathrochelates with with Regard Regard to to the the Hydrogen Hydrogen Evolution Evolution Reaction Reaction in in Th. **2018**. https://doi.org/10.5772/intechopen.80267.
(33) Lacy, D. C.; Roberts, G. M.; Peters, J. C.; Lacy, D. C.; Roberts, G. M.; Peters, J. C. The Cobalt Hydride That Never Was : Revisiting Schrauzer ' s " Hydridocobaloxime " The Cobalt Hydride That Never Was : Revisiting Schrauzer ' s " Hydridocobaloxime ." **2015**. https://doi.org/10.1021/jacs.5b01838.
(34) Cramer, C. J. *Essentials of Computational Chemistry: Theories and Models*, 2nd ed.; Wiley: West Sussex, 2004.
(35) Gong, W.; Xie, Y.; Pham, T. D.; Shetty, S.; Son, F. A.; Idrees, K. B.; Chen, Z.; Xie, H.; Liu, Y.; Snurr, R. Q.; et al. Creating Optimal Pockets in a Clathrochelate-Based Metal–Organic Framework for Gas Adsorption and Separation: Experimental and Computational Studies. *J. Am. Chem. Soc.* **2022**, *144* (8), 3737–3745. https://doi.org/10.1021/jacs.2c00011.
(36) Makkar, P.; Ghosh, N. N. A Review on the Use of DFT for the Prediction of the Properties of Nanomaterials. *RSC Adv.* **2021**, *11* (45), 27897–27924. https://doi.org/10.1039/D1RA04876G.
(37) Dinh Nguyen, M. T.; Ranjbari, A.; Catala, L.; Brisset, F.; Millet, P.; Aukauloo, A. Implementing Molecular Catalysts for Hydrogen Production in Proton Exchange Membrane Water Electrolysers. *Coord. Chem. Rev.* **2012**, *256* (21–22), 2435–2444. https://doi.org/10.1016/j.ccr.2012.04.040.
(38) Thu, M.; Nguyen, D.; Charlot, M.; Aukauloo, A. Structural, Electronic, and Theoretical Description of a Series of Cobalt Clathrochelate Complexes in the Co (III), Co (II) and Co (I) Oxidation States. **2011**, No. Iii, 911–922.
(39) Dreimann, J. M.; Kohls, E.; Warmeling, H. F. W.; Stein, M.; Guo, L. F.; Garland, M.; Dinh, T. N.; Vorholt, A. J. In Situ Infrared Spectroscopy as a Tool for Monitoring Molecular Catalyst for Hydroformylation in Continuous Processes. *ACS Catal.* **2019**, *9* (5), 4308–4319. https://doi.org/10.1021/acscatal.8b05066.
(40) Song, X.; Xu, L.; Sun, X.; Han, B. In Situ/Operando Characterization Techniques for Electrochemical CO2 Reduction. *Sci. China Chem.* **2023**, *66* (2), 315–323. https://doi.org/10.1007/s11426-021-1463-6.
(41) Samajdar, R. N.; Brown, S. A.; Kairy, S. K.; Robertson, S. D.; Wain, A. J. Methodologies for Operando ATR-IR Spectroscopy of Magnesium Battery Electrolytes. *Anal. Chem.* **2022**, *94*

(43), 14985–14993. https://doi.org/10.1021/acs.analchem.2c02843.
(42) Ganesan, A.; Zimudzi, T. J.; Hall, D. M. Characterizing Working Electrodes for In-Operando Spectroelectrochemical Cells Using Electrochemical Impedance Spectroscopy. *ECS Meet. Abstr.* **2022**, *MA2022-02* (1), 92. https://doi.org/10.1149/MA2022-02192mtgabs.
(43) Gordon, M. S.; Schmidt, M. W. Advances in Electronic Structure Theory: GAMESS a Decade Later. In *Theory and Applications of Computational Chemistry The First Forty Years*; Dykstra, C. E., Frenking, G., Kim, K. S., Scuseria, G. E., Eds.; Elsevier Science, 2005; pp 1185–1189. https://doi.org/https://doi.org/10.1016/B978-044451719-7/50084-6.
(44) Schmidt, M. W.; Baldridge, K. K.; Boatz, J. A.; Elbert, S. T.; Gordon, M. S.; Jensen, J. H.; Koseki, S.; Matsunaga, N.; Nguyen, K. A.; Su, S.; et al. General Atomic and Molecular Electronic Structure System. *J. Comput. Chem.* **1993**, *14* (11), 1347–1363. https://doi.org/10.1002/jcc.540141112.
(45) Hay, P. J.; Wadt, W. R.; Hay, P. J.; Wadt, W. R. Ab Initio Effective Core Potentials for Molecular Calculations . Potentials for the Transition Metal Atoms Sc to Hg Ab Initio Effective Core Potentials for Molecular Calculations . Potentials for the Transition Metal Atoms Sc to Hg. **1985**, *270*. https://doi.org/10.1063/1.448799.
(46) Marenich, A. V.; Cramer, C. J.; Truhlar, D. G. Universal Solvation Model Based on Solute Electron Density and on a Continuum Model of the Solvent Defined by the Bulk Dielectric Constant and Atomic Surface Tensions. *J. Phys. Chem. B* **2009**, *113* (18), 6378–6396. https://doi.org/10.1021/jp810292n.
(47) Lebed, E. G.; Belov, A. S.; Dolganov, A. V; Vologzhanina, A. V; Szebesczyk, A.; Gumienna-kontecka, E.; Kozlowski, H.; Bubnov, Y. N.; Dubey, I. Y.; Voloshin, Y. Z. First Clathrochelate Iron and Cobalt (II) Tris-Dioximates with Reactive Apical Substituents. *Inorg. Chem. Commun.* **2013**, *30*, 53–57. https://doi.org/10.1016/j.inoche.2013.01.020.
(48) Voloshin, Y. Z.; Lebedev, A. Y.; Novikov, V. V; Dolganov, A. V; Vologzhanina, A. V; Lebed, E. G.; Pavlov, A. A.; Starikova, Z. A.; Buzin, M. I.; Bubnov, Y. N. Template Synthesis , X-Ray Structure, Spectral and Redox Properties of the Paramagnetic Alkylboron-Capped Cobalt (II) Clathrochelates and Their Diamagnetic Iron (II) -Containing Analogs. *Inorganica Chim. Acta* **2013**, *399*, 67–78. https://doi.org/10.1016/j.ica.2012.12.042.
(49) Belov, A. S.; Zelinskii, G. E.; Varzatskii, O. A.; Belaya, I. G.; Vologzhanina, A. V; Dolganov, A. V; Novikov, V. V; Voloshin, Y. Z. Molecular Design of Cage Iron(II) and Cobalt(II,III) Complexes with a Second Fluorine-Enriched Superhydrophobic Shell. *Dalt. Trans.* **2015**, *3*, 3773–3784. https://doi.org/10.1039/c4dt03628j.
(50) Novikov, V. V; Ananyev, I. V; Pavlov, A. A.; Fedin, M. V; Lyssenko, K. A.; Voloshin, Y. Z. Spin-Crossover Anticooperativity Induced by Weak Intermolecular Interactions. *J. Phys. Chem. Lett.* **2014**, *5*, 496–500.
(51) Allouche, A.-R. Gabedit—A Graphical User Interface for Computational Chemistry Softwares. *J. Comput. Chem.* **2010**, *32* (1), 174–182. https://doi.org/10.1002/jcc.
(52) Pápai, M.; Vankó, G. On Predicting Mossbauer Parameters of Iron-Containing Molecules with Density-Functional Theory. *J. Chem. Theory Comput.* **2013**, *9*, 5004−5020.
(53) Isse, A. A.; Gennaro, A. Absolute Potential of the Standard Hydrogen Electrode and the Problem of Interconversion of Potentials in Different Solvents. *J. Phys. Chem. B* **2010**, *114*, 7894–7899.
(54) Donald, W. A.; Leib, R. D.; Demireva, M.; Brien, J. T. O.; Prell, J. S.; Williams, E. R. Directly Relating Reduction Energies of Gaseous Eu(H2O)N3+, n = 55-140, to Aqueous Solution: The Absolute SHE Potential and Real Proton Solvation Energy. *J. Am. Chem. Soc.* **2009**, *131*, 13328–13337.
(55) Fu, Y.; Liu, L.; Yu, H.; Wang, Y.; Guo, Q. Quantum-Chemical Predictions of Absolute Standard Redox Potentials of Diverse Organic Molecules and Free Radicals in Acetonitrile. *J. Am. Chem. Soc.* **2005**, No. 9, 7227–7234.
(56) Lewis, A.; Bumpus, J. A.; Truhlar, D. G.; Cramer, C. J. Molecular Modeling of Environmentally Important Processes: Reduction Potentials. *J. Chem. Educ.* **2004**, *81* (4),

596–604. https://doi.org/10.1021/ed081p596.
(57) Ho, J. Are Thermodynamic Cycles Necessary for Continuum Solvent Calculation of PKas and Reduction Potentials? *Phys. Chem. Chem. Phys.* **2015**, *17*, 2859–2868. https://doi.org/10.1039/c4cp04538f.
(58) Hughes, T. F.; Friesner, R. A. Development of Accurate DFT Methods for Computing Redox Potentials of Transition Metal Complexes : Results for Model Complexes and Application to Cytochrome P450. *J. Chem. Theory. Comput.* **2012**, *8*, 442−459. https://doi.org/10.1021/ct2006693.
(59) Kirby, F.; Burnea, B.; Shi, H.; Ko, K. C.; Lee, J. Y. Reduction Potential Tuning of Fi Rst Row Transition Metal M III / M II (M = Cr, Mn, Fe, Co, Ni) Hexadentate Complexes for Viable Aqueous Redox Fl Ow Battery Catholytes : A DFT Study. *Electrochim. Acta* **2017**, *246*, 156–164. https://doi.org/10.1016/j.electacta.2017.05.199.
(60) Balatskiy, D. V.; Chuprin, A. S.; Dudkin, S. V.; Desdin-Garcia, L. F.; Corcho-valdes, A. L.; Antuch, M.; Buznik, V. M.; Bratskaya, S. Y.; Voloshin, Y. Z. 57Fe Mossbauer and DFT Study of the Electronic and Spatial Structures of the Iron (II) (Pseudo) Clathrochelates: The Effect of Ligand Field. *Phys. Chem. Chem. Phys.* **2023**, *25*, 18679–18690. https://doi.org/10.1039/D3CP01887C.
(61) Solis, B. H.; Hammes-Schiffer, S. Proton-Coupled Electron Transfer in Molecular Electrocatalysis : Theoretical Methods and Design Principles. *Inorg. Chem.* **2014**, *53*, 6427–6443.
(62) Solis, B. H.; Hammes-Schiffer, S. Theoretical Analysis of Mechanistic Pathways for Hydrogen Evolution Catalyzed by Cobaloximes. *Inorg. Chem.* **2011**, *50* (21), 11252–11262. https://doi.org/10.1021/ic201842v.
(63) Zigler, D. F.; Morseth, Z. A.; Wang, L.; Ashford, D. L.; Brennaman, M. K.; Grumstrup, E. M.; Brigham, E. C.; Gish, M. K.; Dillon, R. J.; Alibabaei, L. et al. Disentangling the Physical Processes Responsible for the Kinetic Complexity in Interfacial Electron Transfer of Excited Ru(II) Polypyridyl Dyes on TiO2. *J. Am. Chem. Soc.* **2016**, *138*, 4426–4438. https://doi.org/10.1021/jacs.5b12996.
(64) Skara, G.; Gimferrer, M.; Proft, F. De; Salvador, P.; Pinter, B. Scrutinizing the Noninnocence of Quinone Ligands in Ruthenium Complexes: Insights from Structural, Electronic, Energy, and E Ff Ective Oxidation State Analyses. *Inorg. Chem.* **2016**, *55*, 2185−2199. https://doi.org/10.1021/acs.inorgchem.5b02543.
(65) Grelaud, G.; Gauthier, N.; Luo, Y.; Paul, F.; Fabre, B.; Barrière, F.; Ababou-Girard, S.; Roisnel, T.; Humphrey, M. G. Redox-Active Molecular Wires Derived from Dinuclear Ferrocenyl/ Ruthenium(II) Alkynyl Complexes: Covalent Attachment to Hydrogen-Terminated Silicon Surfaces. *J. Phys. Chem. C* **2014**, *118* (7), 3680–3695. https://doi.org/10.1021/jp412498t.
(66) Panetier, J. A.; Letko, C. S.; Tilley, T. D.; Head-Gordon, M. Computational Characterization of Redox Non-Innocence in Cobalt-Bis(Diaryldithiolene)-Catalyzed Proton Reduction. *J. Chem. Theory Comput.* **2016**, *12*, 223–230. https://doi.org/10.1021/acs.jctc.5b00968.
(67) Antuch, M.; Millet, P. The Use of Density Functional Theory to Decipher the Electrochemical Activity of Metal Clathrochelates with Regard to the Hydrogen Evolution Reaction in the Homogeneous Phase. In *Density Functional Theory*; Glossman-Mitnik, D., Ed.; IntechOpen, 2018; pp 75–89. https://doi.org/10.5772/intechopen.80267.